Publisher: GSA
Journal: GEOL: Geology
DOI:10.1130/G38432.1

Isotopic signature of dissolved iron delivered to the Southern Ocean from hydrothermal vents in the East Scotia Sea

Jessica K. Klar[1,2*], Rachael H. James[1], Dakota Gibbs[3,4], Alastair Lough[1], Ian Parkinson[5], J. Andrew Milton[1], Jeffrey A. Hawkes[6], and Douglas P. Connelly[2]

[1]*Ocean and Earth Science, University of Southampton Waterfront Campus, National Oceanography Centre Southampton, European Way, Southampton SO14 3ZH, UK*

[2]*Now at: LEGOS, University of Toulouse, IRD, CNES, CNRS, UPS, 18 av. Edouard Belin, 31401 Toulouse, France*

[3]*Marine Geosciences, National Oceanography Centre Southampton, European Way, Southampton SO14 3ZH, UK*

[4]*Southern Cross Geoscience, Military Road, Lismore, NSW 2480, Australia*

[5]*School of Earth Sciences, University of Bristol, Queens Road, Bristol, BS8 1RJ, UK*

[6]*Department of Chemistry, Uppsala University, SE-751 05 Uppsala, Sweden*

*E-mail address: Jessica.klar@legos.obs-mip.fr

ABSTRACT

It has recently been demonstrated that hydrothermal vents are an important source of dissolved Fe (dFe) to the Southern Ocean. The isotopic composition (δ^{56}Fe) of dFe in vent fluids appears to be distinct from other sources of dFe to the deep ocean, but the evolution of δ^{56}Fe during mixing between vent fluids and seawater is poorly constrained. Here we present the evolution of δ^{56}Fe for dFe in hydrothermal fluids and dispersing plumes from two sites in the East Scotia Sea. We show that δ^{56}Fe values in the buoyant plume are distinctly lower (as low as −1.19 ‰) than the hydrothermal fluids (−0.29 ‰), attributed to (i) precipitation of Fe-sulfides in the early stages of mixing, and (ii) partial oxidation of Fe(II) to Fe(III), > 55 % of which subsequently precipitates as Fe-oxyhydroxides. By contrast, the δ^{56}Fe signature of stabilized dFe in the neutrally buoyant plume is –0.3 to –0.5 ‰. This cannot be explained by continued dilution of the buoyant plume with background seawater; rather, we suggest that isotope fractionation of dFe occurs during plume dilution due to Fe ligand complexation and exchange with labile particulate Fe. The δ^{56}Fe signature of stabilized hydrothermal dFe in the East Scotia Sea is distinct from background seawater and may be used to quantify the hydrothermal dFe input to the ocean interior.

INTRODUCTION

The Southern Ocean is of significant importance to the global carbon cycle and it is a major sink for atmospheric carbon dioxide (CO_2) (Pollard et al., 2009). The micronutrient iron (Fe) is a key regulator of primary productivity and therefore CO_2 uptake in the Southern Ocean (e.g., Martin et al., 1990). The impact of past and future climate variability has been shown to be mediated by modifications to the supply of Fe to the biota in this area (e.g., Watson et al., 2000). Understanding the pathways that govern Fe supply and removal to/from the Southern Ocean is therefore critical to quantifying the impact of Fe on global productivity. However, the relative importance of different sources of Fe to the oceans is not well known, and flux estimates from atmospheric dust, hydrothermal vents, icebergs and oceanic sediments vary by orders of magnitude (Boyd and Ellwood, 2010).

A number of recent studies have demonstrated that as much as 46 % of hydrothermal Fe may remain in the dissolved (< 0.2 μm) phase, in the form of either colloids or organic complexes (Bennett et al., 2008; Hawkes et al., 2013; Saito et al., 2013; Fitzsimmons et al., 2014; Hawkes et al., 2014; Kleint et al., 2016). In support of this, modeling studies have shown that observations of the distribution of dissolved Fe (dFe) in the Southern Ocean can only be replicated when the Fe flux from hydrothermal sources is included (Tagliabue et al., 2014; Tagliabue et al., 2010) and analyses of dFe on transects across the North Atlantic, South Atlantic and Eastern Equatorial Pacific have provided evidence for advection of hydrothermal dFe for some thousands of kilometers away from the mid-ocean ridge (Saito et al., 2013; Conway and John, 2014; Fitzsimmons et al., 2014; Resing et al., 2015).

Attempts have been made to parameterize hydrothermal dFe using dissolved $Fe/^{3}He$ ratios, but this approach is imprecise because hydrothermal fluids have widely variable $Fe/^{3}He$ (Tagliabue et al., 2010; Saito et al., 2013). Moreover, the controls on the proportion of hydrothermal Fe that is stabilized in the dissolved phase are unknown (Kleint et al., 2016). In principle, one way to circumvent some of these problems is by analysis of stable Fe isotopes. However, $\delta^{56}Fe$ values of dFe ($\delta^{56}Fe$, where $\delta^{56}Fe = [(^{56}Fe/^{54}Fe)_{sample}/(^{56}Fe/^{54}Fe)_{IRMM\text{-}14} - 1] \times 1000$) proximal to vent sites varies from −1.35 ‰ to +0.56 ‰ (Conway and John, 2014; Fitzsimmons et al., 2016), whereas $\delta^{56}Fe$ values reported for hydrothermal fluids range from −0.69 to +0.28 ‰ (Beard et al., 2003; Severmann et al., 2004; Rouxel et al., 2008; Bennett et al., 2009; Rouxel et al., 2016). The likely reason for this is that the $\delta^{56}Fe$ composition of hydrothermal dFe is modified on mixing with seawater due to precipitation of Fe sulfides, oxidation of Fe(II) to Fe(III) and Fe(III)-oxyhydroxide formation (e.g., Welch et al., 2003; Rouxel et al., 2008; Bennett et al., 2009; Roy et al., 2012; Rouxel et al., 2016).

Here we study the evolution of $\delta^{56}Fe$ during mixing between hydrothermal fluids and seawater, presenting the first compilation of $\delta^{56}Fe$ in hydrothermal fluids, buoyant and non-buoyant plumes at two vent sites, E2 and E9N, located on the East Scotia Ridge (ESR) (see supplementary information for sample site descriptions and

Publisher: GSA
Journal: GEOL: Geology
DOI:10.1130/G38432.1
sampling strategies). We use these data to determine the controls on the isotopic signature of hydrothermal dFe delivered to the Scotia Sea in the Southern Ocean and show that Fe isotopes are likely to be an effective tracer of hydrothermal dFe throughout most parts of the world's ocean.

RESULTS

Vent fluids with minimal seawater mixing (Mg < 1.64 mM) display Fe concentrations of 1070 μM at E2 and 580 μM at E9N and have similar δ^{56}Fe values (−0.28 ‰ at E2 and −0.30 ‰ at E9N). Water samples obtained from the buoyant part of the hydrothermal plume have lowest δ^{56}Fe values (as low as −1.19 ‰ at E2 and as low as −0.76 ‰ at E9N) and highest dFe concentrations (up to 83.5 nM at E2 and up to 23.0 nM at E9N; Fig. 1). As the hydrothermal plume is dispersed and further diluted in the neutrally buoyant part of the hydrothermal plume, dFe concentrations decrease whereas δ^{56}Fe values increase. Slight differences in δ^{56}Fe values and dFe concentrations can be observed between the two vent sites: for the same degree of dilution, samples from E9N tend to have slightly higher δ^{56}Fe and lower dFe compared to samples from E2. Total (dissolved + particulate) concentrations of Fe (tFe) are, on average, 40 ± 10 % and 70 ± 30 % lower at, respectively, E2 and E9N, than calculated assuming Fe is conserved during mixing between the endmember vent fluid and seawater (Fig. 1). Partitioning of Fe between different size fractions, and δ^{56}Fe values, may, however, be slightly modified in the interval between sampling and processing (see Supplementary Information).

DISCUSSION

The 'missing' tFe is likely to have been removed by precipitation of iron sulfides immediately on venting at the seafloor (e.g., Rudnicki and Elderfield, 1993) and higher Fe-sulfide removal at E9N may be due to the slightly higher sulfide concentrations found in E9N vent fluids (James et al., 2014). Field and experimental studies have shown that light Fe isotopes are preferentially incorporated into Fe-sulfides, leaving the remaining dFe isotopically heavy (Rouxel et al., 2008; Bennett et al., 2009; Roy et al., 2012; Rouxel et al., 2016). Assuming that the fractionation factor associated with Fe-sulfide formation ($\Delta_{Fe(II)\text{-}FeS}$) is +0.66 ‰ (Rouxel et al., 2008; Bennett et al., 2009; Roy et al., 2012), then according to the Rayleigh fractionation model the δ^{56}Fe value of the remaining dFe would be +0.07 ± 0.05 ‰ at E2 and +0.49 ± 0.05 ‰ at E9N. Assuming a small part (< 10 %) of the dFe in the buoyant plume may be present as pyrite nanoparticles (Yücel et al., 2011) that would contribute light isotopes to the dissolved fraction, this would still produce δ^{56}Fe values (−0.02 ‰ at E2; +0.39 ‰ at E9N) that are higher than we measure in the buoyant plumes

The low Fe isotopic values in the buoyant part of the plume are however consistent with Fe-sulfide formation combined with partial oxidation of Fe(II) to Fe(III). Oxidation of Fe(II) to Fe(III) results in enrichment of the heavy Fe isotopes in Fe(III) such that the δ^{56}Fe value of the remaining Fe(II) is up to 3.56 ‰ lower than the Fe(III) (Welch et al., 2003). Fe(III) is not stable in seawater and rapidly forms Fe(III)-oxyhydroxides, which tend to aggregate and coagulate into larger particles (Field and Sherrell, 2000; Statham et al., 2005). As these ‘heavy’ Fe(III)-oxyhydroxide particles are no longer part of the dFe fraction (< 0.2 μm), the δ^{56}Fe value of the remaining dFe pool decreases (e.g., Severmann et al., 2004; Bennett et al., 2009; Rouxel et al., 2016).

The evolution of δ^{56}Fe in the buoyant plumes at E2 and E9N after sulfide formation is complete can therefore be modelled as a function of the proportion of Fe(II) oxidized to Fe(III) and the proportion of Fe(III) that leaves the dissolved phase (i.e., coagulates to form particles larger than 0.2 μm) (Fig. 2; see Supplementary

DOI:10.1130/G38432.1

Information for a detailed description). According to the model, the δ^{56}Fe values measured in the buoyant plume are consistent with oxidation of 30 – 75 % of Fe(II) to Fe(III), with removal of > 50 % of the Fe(III) produced, at both E2 and E9N. The average proportion of tFe present as dFe in the buoyant plume (~50 %; Fig. 1) is also consistent with the modeled amount of Fe(III) precipitation.

As the plume moves upwards through the water column it continues to mix with seawater until the density within the plume equals that of surrounding seawater, at which point it spreads out to form the neutrally buoyant plume. During this process, dFe decreases and δ^{56}Fe increases. The most dilute part of the neutrally buoyant plume sampled at E2 has dFe ≈15 nM and δ^{56}Fe ≈ –0.5 ‰; at E9N dFe ≈ 7 nM and δ^{56}Fe ≈ –0.3 ‰. By contrast, background seawater (Weddell Sea Deep Water) has dFe ≈ 0.7 nM and δ^{56}Fe ≈ –0.15 ‰ (Abadie et al., 2013). However, although the decrease in dFe concentrations in the neutrally buoyant plume is broadly consistent with simple mixing between the buoyant plume and surrounding seawater, mixing cannot explain the evolution of δ^{56}Fe as measured δ^{56}Fe values are higher than predicted (Fig. 3).

Relatively high δ^{56}Fe values cannot be attributed to limited fallout of Fe-sulfide nanoparticles (Yücel et al., 2011), as these would have to have unrealistically low δ^{56}Fe (< –7.5 ‰) to reproduce the δ^{56}Fe values we measure for dFe in the neutrally buoyant plume. Our data therefore imply that a small proportion of hydrothermal Fe is stabilized within the < 0.2 μm size fraction. This Fe could be in the form of colloidal Fe-oxyhydroxides and/or Fe-sulfide nanoparticles, or Fe complexed by ligands (FeL) (Yücel et al., 2011; Hawkes et al., 2013; Fitzsimmons et al., 2016). Studies of Fe speciation in the neutrally buoyant plumes from the ESR indicate that ~50 % of dFe is in the colloidal fraction and ~30 % of dFe is in the form of FeL (Hawkes et al., 2013). Relatively high δ^{56}Fe values in the neutrally buoyant plume may therefore reflect exchange between these dFe species, and labile Fe in the particulate fraction (e.g., neo-formed FeOOH particles, adsorbed Fe) (e.g., Ellwood et al., 2015).

IMPLICATIONS

Our data demonstrate that the δ^{56}Fe value of hydrothermal Fe stabilized in the dissolved fraction and delivered to the East Scotia Sea in the Southern Ocean is –0.5 ‰ (E2) and –0.3 ‰ (E9N), significantly higher than the value assigned (–1.35 ‰) in a recent study that aimed to quantify dissolved Fe sources to a North Atlantic transect (Conway and John, 2014). Our work shows that this value is critically dependent on the δ^{56}Fe value of the hydrothermal fluid, but also on the proportion of the Fe that precipitates as sulfides immediately on venting; the higher this is (e.g., E9N), the higher the δ^{56}Fe value of the stabilized dFe. Nevertheless, the δ^{56}Fe value of stabilized hydrothermal Fe from both vent sites in the East Scotia Sea is distinct from the background seawater (Weddell Sea Deep Water), as well as from other water masses surrounding the world's mid-ocean ridges, and from other deep ocean Fe sources (Fig. 4). There is however potential for overlap with the δ^{56}Fe signature of Fe derived from reducing sediments.

While our study confirms the importance of sulfide precipitation and Fe oxidation for setting the δ^{56}Fe value of hydrothermal iron delivered to the ocean interior, it also reveals the possibility for Fe-L complexation and continued exchange of Fe between dFe and particulate Fe. Understanding the physico-chemical speciation of dFe remains essential for quantifying the longevity of hydrothermal iron plumes and for modeling climate.

ACKNOWLEDGMENTS

This work was supported by UK Natural Environment Research Council (NERC) National Capability funds and the Graduate School of the National Oceanography Centre Southampton. Research cruises JC042 and JC055 were funded by NERC consortium grant NE/D01249X/1. We are thankful for the support of the Captain and crew of RRS *James Cook* on both cruises. We also thank D. Green and B. Alker for both ship-board and onshore laboratory assistance. We thank K. Nakamura for the loan of his Eh sensor, and two anonymous reviewers for their considered and constructive reviews.

REFERENCES CITED

Abadie, C., Lacan, F., Radic, A., and Poitrasson, F., 2013, Dissolved and particulate iron concentrations and isotopic compositions in the South Atlantic and Southern Ocean: Mineralogical Magazine, v. 77, p. 551.

Beard, B.L., Johnson, C.M., Von Damm, K.L., and Poulson, R.L., 2003, Iron isotope constraints on Fe cycling and mass balance in oxygenated Earth oceans: Geology, v. 31, p. 629–632, doi:10.1130/0091-7613(2003)031<0629:IICOFC>2.0.CO;2.

Bennett, S.A., Achterberg, E.P., Connelly, D.P., Statham, P.J., Fones, G.R., and German, C.R., 2008, The distribution and stabilisation of dissolved Fe in deep-sea hydrothermal plumes: Earth and Planetary Science Letters, v. 270, p. 157–167, doi:10.1016/j.epsl.2008.01.048.

Bennett, S.A., Rouxel, O., Schmidt, K., Garbe-Schönberg, D., Statham, P.J., and German, C.R., 2009, Iron isotope fractionation in a buoyant hydrothermal plume, 5 degrees S Mid-Atlantic Ridge: Geochimica et Cosmochimica Acta, v. 73, p. 5619–5634, doi:10.1016/j.gca.2009.06.027.

Boyd, P.W., and Ellwood, M.J., 2010, The biogeochemical cycle of iron in the ocean: Nature Geoscience, v. 3, p. 675–682, doi:10.1038/ngeo964.

Conway, T.M., and John, S.G., 2015, The cycling of iron, zinc and cadmium in the North East Pacific Ocean – Insights from stable isotopes: Geochimica et Cosmochimica Acta, v. 164, p. 262–283, doi:10.1016/j.gca.2015.05.023.

Conway, T.M., and John, S.G., 2014, Quantification of dissolved iron sources to the North Atlantic Ocean: Nature, v. 511, p. 212–215, doi:10.1038/nature13482.

Conway, T.M., John, S.G., and Lacan, F., 2016, Intercomparison of dissolved iron isotope profiles from reoccupation of three GEOTRACES stations in the Atlantic Ocean: Marine Chemistry, v. 183, p. 50–61, doi:10.1016/j.marchem.2016.04.007, (erratum available at http://dx.doi.org/10.1016/j.marchem.2016.06.005).

Ellwood, M. J., Hutchins, D. A., Lohan, M. C., Milne, A., Nasemann, P., Nodder, S. D., Sander, S. G., Strzepek, R., Wilhelm, S. W., and Boyd, P. W., 2015, Iron stable isotopes track pelagic iron cycling during a subtropical phytoplankton bloom: Proceedings of the National Academy of Sciences, v. 112, no. 1, p. E15-E20, doi:10.1073/pnas.1421576112.

Field, M.P., and Sherrell, R.M., 2000, Dissolved and particulate Fe in a hydrothermal plume at 9 degrees 45 ’ N, East Pacific Rise: Slow Fe (II) oxidation kinetics in Pacific plumes: Geochimica et Cosmochimica Acta, v. 64, p. 619–628, doi:10.1016/S0016-7037(99)00333-6.

Fitzsimmons, J. N., Boyle, E. A., and Jenkins, W. J., 2014, Distal transport of dissolved hydrothermal iron in the deep South Pacific Ocean: Proceedings of the National Academy of Sciences, v. 111, no. 47, p. 16654-16661, doi:10.1073/pnas.1418778111.

Fitzsimmons, J. N., Conway, T. M., Lee, J. M., Kayser, R., Thyng, K. M., John, S. G., and Boyle, E. A., 2016, Dissolved iron and iron isotopes in the southeastern

Pacific Ocean: Global Biogeochemical Cycles, v. 30, no. 10, p. 1372-1395, doi:10.1002/2015GB005357.

Hawkes, J.A., Connelly, D.P., Gledhill, M., and Achterberg, E.P., 2013, The stabilisation and transportation of dissolved iron from high temperature hydrothermal vent systems: Earth and Planetary Science Letters, v. 375, p. 280–290, doi:10.1016/j.epsl.2013.05.047.

Hawkes, J.A., Connelly, D.P., Rijkenberg, M.J.A., and Achterberg, E.P., 2014, The importance of shallow hydrothermal island arc systems in ocean biogeochemistry: Geophysical Research Letters, v. 41, p. 942–947, doi:10.1002/2013GL058817.

Homoky, W.B., John, S.G., Conway, T.M., and Mills, R.A., 2013, Distinct iron isotopic signatures and supply from marine sediment dissolution: Nature Communications, v. 4, p. 2143, doi:10.1038/ncomms3143.

Homoky, W.B., Severmann, S., Mills, R.A., Statham, P.J., and Fones, G.R., 2009, Pore-fluid Fe isotopes reflect the extent of benthic Fe redox recycling: Evidence from continental shelf and deep-sea sediments: Geology, v. 37, p. 751–754, doi:10.1130/G25731A.1.

James, R. H., Green, D. R. H., Stock, M. J., Alker, B. J., Banerjee, N. R., Cole, C., German, C. R., Huvenne, V. A. I., Powell, A. M., and Connelly, D. P., 2014, Composition of hydrothermal fluids and mineralogy of associated chimney material on the East Scotia Ridge back-arc spreading centre: Geochimica et Cosmochimica Acta, v. 139, no. 0, p. 47-71, doi:10.1016/j.gca.2014.04.024

John, S.G., and Adkins, J., 2012, The vertical distribution of iron stable isotopes in the North Atlantic near Bermuda: Global Biogeochemical Cycles, v. 26, GB2034, doi:10.1029/2011GB004043.

Kleint, C., Hawkes, J.A., Sander, S.G., and Koschinsky, A., 2016, Voltammetric Investigation of Hydrothermal Iron Speciation: Frontiers in Marine Science, v. 3, p. 75, doi:10.3389/fmars.2016.00075, doi:10.3389/fmars.2016.00075.

Labatut, M., Lacan, F., Pradoux, C., Chmeleff, J., Radic, A., Murray, J.W., Poitrasson, F., Johansen, A.M., and Thil, F., 2014, Iron sources and dissolved-particulate interactions in the seawater of the Western Equatorial Pacific, iron isotope perspectives: Global Biogeochemical Cycles, v. 28, p. 1044–1065, doi:10.1002/2014GB004928.

Lacan, F., Radic, A., Jeandel, C., Poitrasson, F., Sarthou, G., Pradoux, C., and Freydier, R., 2008, Measurement of the isotopic composition of dissolved iron in the open ocean: Geophysical Research Letters, v. 35, p. L24610, doi:10.1029/2008GL035841.

Martin, J.H., Fitzwater, S.E., and Gordon, R.M., 1990, Iron deficiency limits phytoplankton growth in Antarctic waters: Global Biogeochemical Cycles, v. 4, p. 5–12, doi:10.1029/GB004i001p00005.

Pollard, R.T., et al., 2009, Southern Ocean deep-water carbon export enhanced by natural iron fertilization: Nature, v. 457, p. 577–580, doi:10.1038/nature07716.

Radic, A., Lacan, F., and Murray, J.W., 2011, Iron isotopes in the seawater of the equatorial Pacific Ocean: New constraints for the oceanic iron cycle: Earth and Planetary Science Letters, v. 306, p. 1–10, doi:10.1016/j.epsl.2011.03.015.

Resing, J.A., Sedwick, P.N., German, C.R., Jenkins, W.J., Moffett, J.W., Sohst, B.M., and Tagliabue, A., 2015, Basin-scale transport of hydrothermal dissolved metals across the South Pacific Ocean: Nature, v. 523, no. 7559, p. 200–203, doi:10.1038/nature14577.

Rouxel, O., Shanks, W.C., Bach, W., and Edwards, K.J., 2008, Integrated Fe- and S-isotope study of seafloor hydrothermal vents at East Pacific rise 9–10 degrees N: Chemical Geology, v. 252, p. 214–227, doi:10.1016/j.chemgeo.2008.03.009.

Rouxel, O., Toner, B. M., Manganini, S. J., and German, C. R., 2016, Geochemistry and iron isotope systematics of hydrothermal plume fall-out at East Pacific Rise 9°50′N: Chemical Geology, v. 441, p. 212-234, doi:10.1016/j.chemgeo.2016.08.027.

Roy, M., Rouxel, O., Martin, J.B., and Cable, J.E., 2012, Iron isotope fractionation in a sulfide-bearing subterranean estuary and its potential influence on oceanic Fe isotope flux: Chemical Geology, v. 300–301, p. 133–142, doi:10.1016/j.chemgeo.2012.01.022.

Rudnicki, M.D., and Elderfield, H., 1993, A chemical model of the buoyant and neutrally buoyant plume above the TAG vent field, 26 degrees N, Mid-Atlantic Ridge: Geochimica et Cosmochimica Acta, v. 57, p. 2939–2957, doi:10.1016/0016-7037(93)90285-5.

Saito, M.A., Noble, A.E., Tagliabue, A., Goepfert, T.J., Lamborg, C.H., and Jenkins, W.J., 2013, Slow-spreading submarine ridges in the South Atlantic as a significant oceanic iron source: Nature Geoscience, v. 6, p. 775–779, doi:10.1038/ngeo1893.

Severmann, S., Johnson, C.M., Beard, B.L., German, C.R., Edmonds, H.N., Chiba, H., and Green, D.R.H., 2004, The effect of plume processes on the Fe isotope composition of hydrothermally derived Fe in the deep ocean as inferred from the Rainbow vent site, Mid-Atlantic Ridge, 36 degrees 14′ N: Earth and Planetary Science Letters, v. 225, p. 63–76, doi:10.1016/j.epsl.2004.06.001.

Severmann, S., McManus, J., Berelson, W.M., and Hammond, D.E., 2010, The continental shelf benthic iron flux and its isotope composition: Geochimica et Cosmochimica Acta, v. 74, p. 3984–4004, doi:10.1016/j.gca.2010.04.022.

Statham, P.J., German, C.R., and Connelly, D.P., 2005, Iron(II) distribution and oxidation kinetics in hydrothermal plumes at the Kairei and Edmond vent sites, Indian Ocean: Earth and Planetary Science Letters, v. 236, p. 588–596, doi:10.1016/j.epsl.2005.03.008.

Tagliabue, A., Aumont, O., and Bopp, L., 2014, The impact of different external sources of iron on the global carbon cycle: Geophysical Research Letters, v. 41, p. 920–926, doi:10.1002/2013GL059059.

Tagliabue, A., Bopp, L., Dutay, J.C., Bowie, A.R., Chever, F., Jean-Baptiste, P., Bucciarelli, E., Lannuzel, D., Remenyi, T., Sarthou, G., Aumont, O., Gehlen, M., and Jeandel, C., 2010, Hydrothermal contribution to the oceanic dissolved iron inventory: Nature Geoscience, v. 3, p. 252–256, doi:10.1038/ngeo818.

Watson, A.J., Bakker, D.C.E., Ridgwell, A.J., Boyd, P.W., and Law, C.S., 2000, Effect of iron supply on Southern Ocean CO2 uptake and implications for glacial atmospheric CO2: Nature, v. 407, p. 730–733, doi:10.1038/35037561.

Welch, S.A., Beard, B.L., Johnson, C.M., and Braterman, P.S., 2003, Kinetic and equilibrium Fe isotope fractionation between aqueous Fe(II) and Fe(III): Geochimica et Cosmochimica Acta, v. 67, p. 4231–4250, doi:10.1016/S0016-7037(03)00266-7.

Yücel, M., Gartman, A., Chan, C.S., and Luther, G., 2011, Hydrothermal vents as a kinetically stable source of iron-sulphide-bearing nanoparticles to the ocean: Nature Geoscience, v. 4, p. 367–371, doi:10.1038/ngeo1148.

FIGURE CAPTIONS

Figure 1. Evolution of dFe, total Fe (tFe = dFe + particulate Fe), calculated tFe (solid black line) and δ^{56}Fe of dFe during mixing (the calculation of the vent fluid (VF) dilution factor is described in the Supplementary Information). The vertical dashed line indicates the approximate boundary between the buoyant plume and the neutrally buoyant plume. Error bars on δ^{56}Fe indicate 2 SD of two replicate analyses or the external reproducibility, whichever is highest. Error bars on the dilution factor are ~14 % (propagated error of the measured dMn concentrations in the plume and background seawater; Table DR3).

Figure 2. Evolution of δ^{56}Fe in the buoyant plume due to oxidation of Fe(II) to Fe(III) as a function of Fe(III) removal from the dissolved phase. Initial dFe(II) composition (after removal of Fe-sulfides) is +0.07 ‰ at E2, and +0.49 ‰ at E9N. Dashed lines represent the isotopic composition of the least dilute sample collected from within the buoyant part of the hydrothermal plume.

Figure 3. Evolution of (a) dFe concentrations and (b) δ^{56}Fe in the neutrally buoyant plume (the calculation of the buoyant plume (BP) dilution factor is described in the Supplementary information). The evolution of dFe and δ^{56}Fe are modeled assuming conservative mixing between the least dilute buoyant plume sample (respectively, 83 nM Fe, –1.2 ‰ for E2 and 23 nM Fe, –0.76 ‰ for E9N) and background seawater (WSDW, 0.7 nM Fe, –0.1 ‰; Abadie et al., 2013).

Figure 4. Range of δ^{56}Fe values of dFe for deep-water sources, compared to δ^{56}Fe values for water masses bathing the world’s mid-ocean ridges. ISOW = Iceland

Publisher: GSA
Journal: GEOL: Geology
DOI:10.1130/G38432.1
Scotland Overflow Water; NADW = North Atlantic Deep Water; AABW = Antarctic Bottom Water; AAIW = Antarctic Intermediate Water; PDW = Pacific Deep Water; UCDW = Upper Circumpolar Deep Water; LCDW = Lower Circumpolar Deep Water. Grey vertical band shows δ^{56}Fe of stabilized dFe supplied from hydrothermal plumes in the East Scotia Sea (–0.5 to –0.3 ‰). Data are from: John and Adkins (2012), Severmann et al. (2010) (reducing sediments); Homoky et al. (2013), Labatut et al. (2014), Radic et al. (2011) (core top/ water column data from within/ above non-reducing sediments); Beard et al. (2003), Bennett et al. (2009), Rouxel et al. (2008), Severmann et al. (2004) (hydrothermal vent fluids); Conway and John (2014), this study (hydrothermal plumes); Conway and John, 2014 (ISOW); Conway and John, 2014, Conway et al. (2016) (NADW); Lacan et al. (2008), Conway et al., 2016 (AABW); Labatut et al. (2014); Radic et al. (2011) (AAIW); Conway and John (2015) (PDW, UCDW, LCDW).

[1]GSA Data Repository item 2016xxx, xxxxxxxx, is available online at http://www.geosociety.org/pubs/ft2016.htm or on request from editing@geosociety.org.

Figure 1

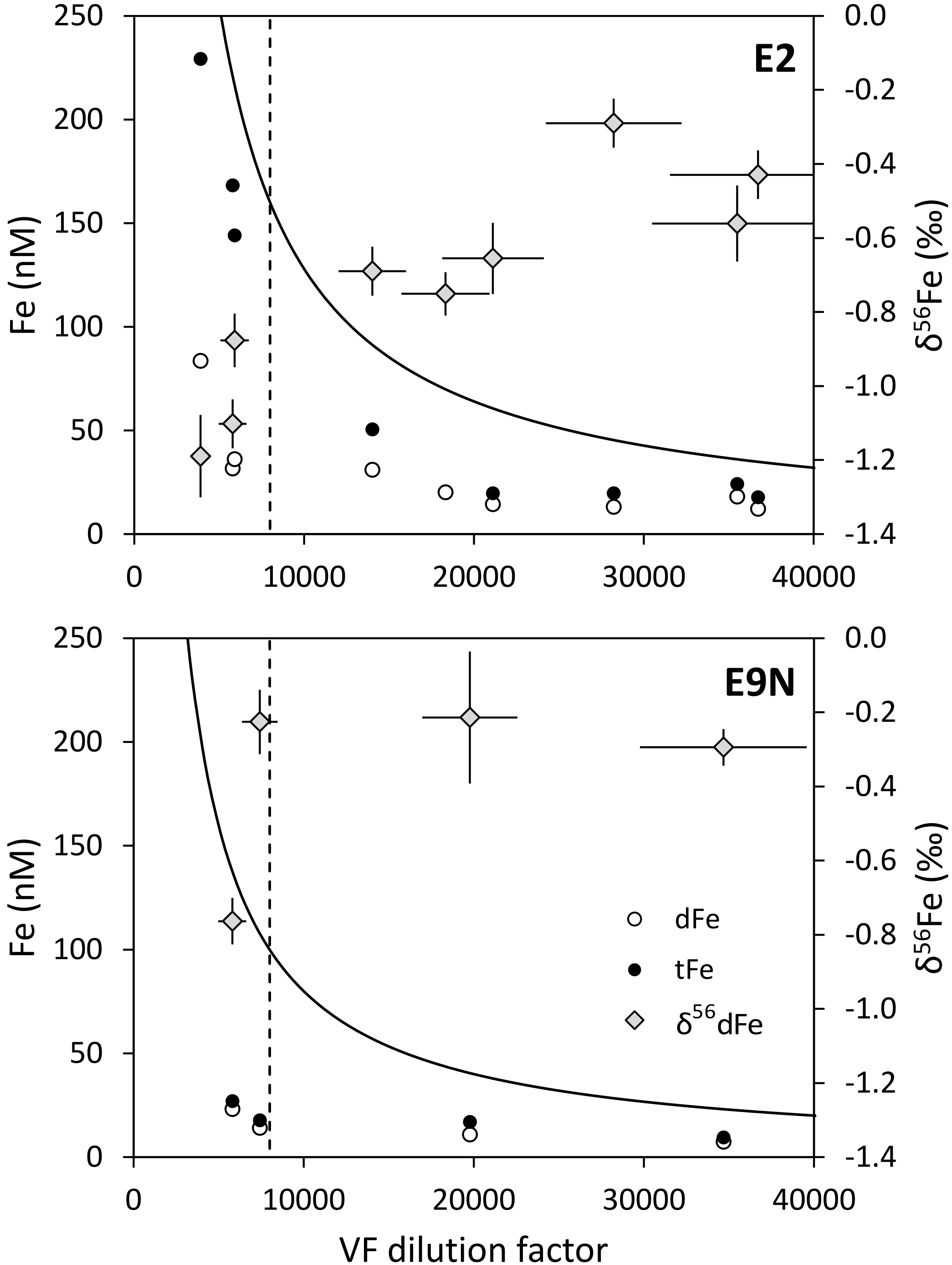
E2
E9N
Fe (nM)
δ56Fe (‰)
VF dilution factor
dFe
tFe
δ56dFe
250
200
150
100
50
0
0.0
-0.2
-0.4
-0.6
-0.8
-1.0
-1.2
-1.4
0
10000
20000
30000
40000

Figure 2

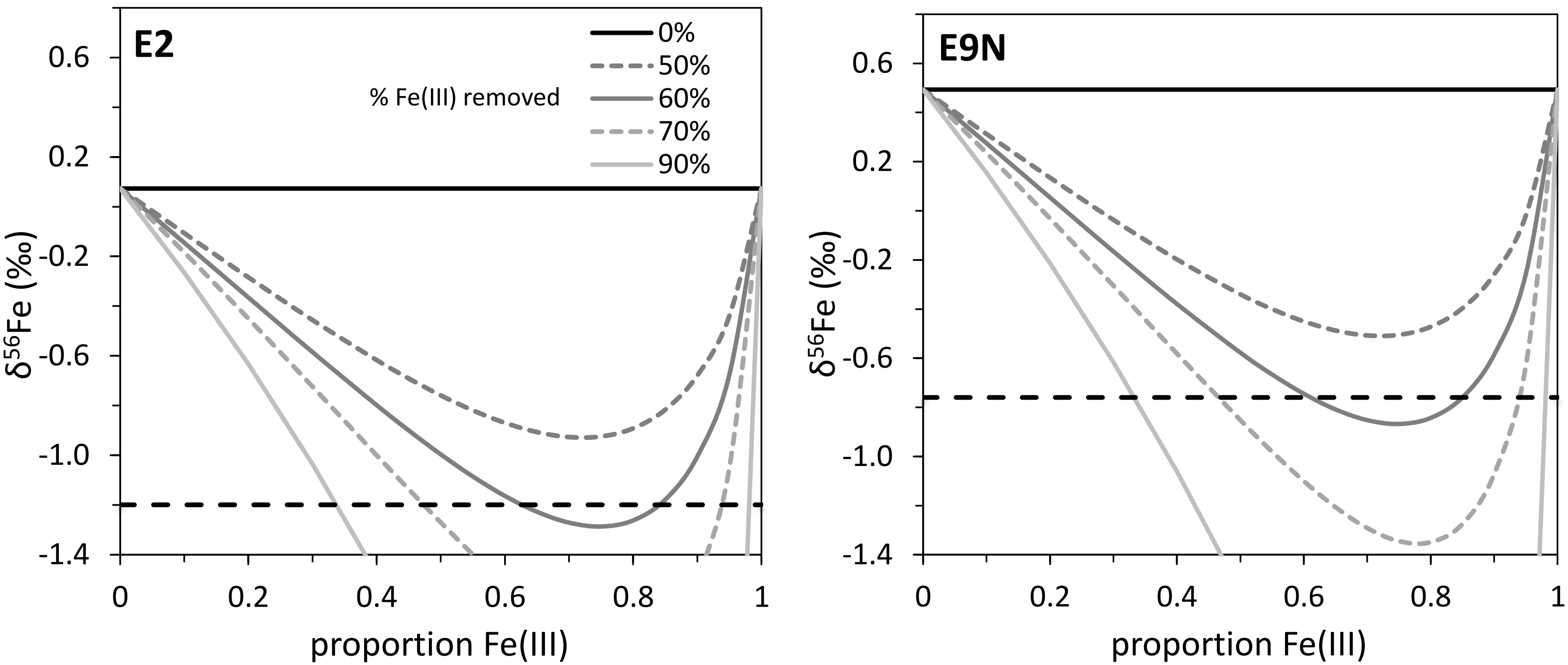
E2
E9N
% Fe(III) removed
0%
50%
60%
70%
90%
δ56Fe (‰)
proportion Fe(III)
0.6
0.2
-0.2
-0.6
-1.0
-1.4
0
0.2
0.4
0.6
0.8
1

Figure 3

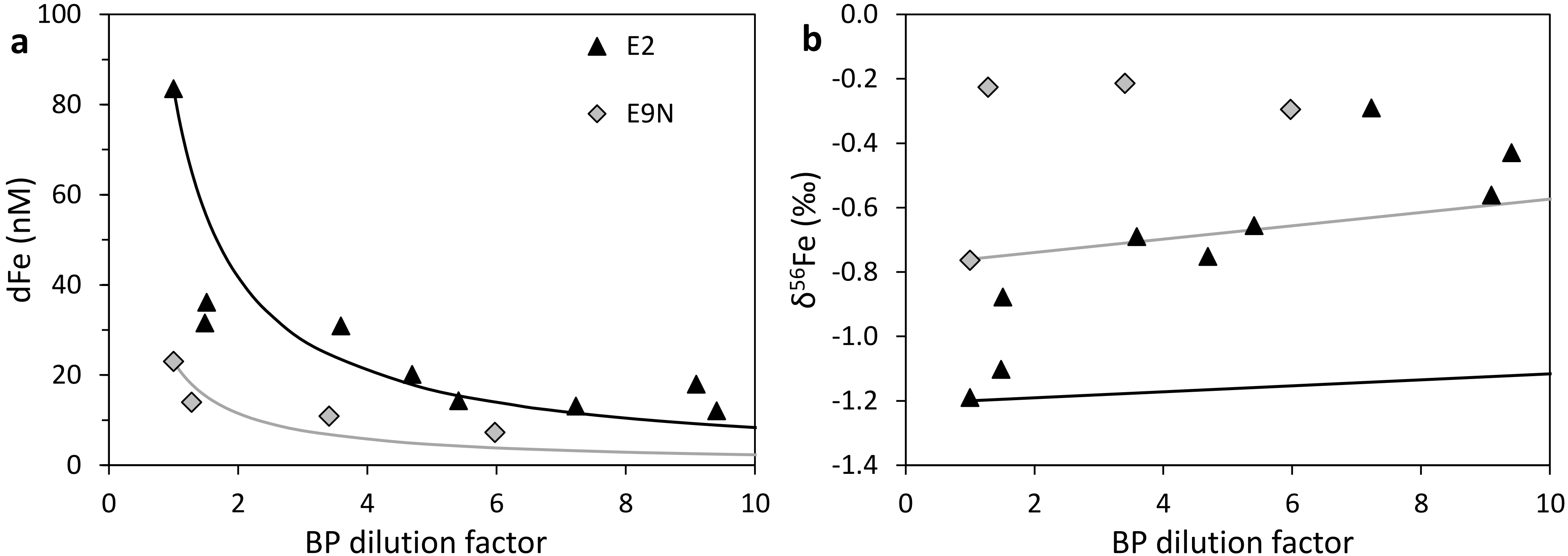
a
b
E2
E9N
100
80
60
40
20
0
dFe (nM)
0
2
4
6
8
10
BP dilution factor
0.0
-0.2
-0.4
-0.6
-0.8
-1.0
-1.2
-1.4
δ56Fe (‰)
0
2
4
6
8
10
BP dilution factor

Figure 4

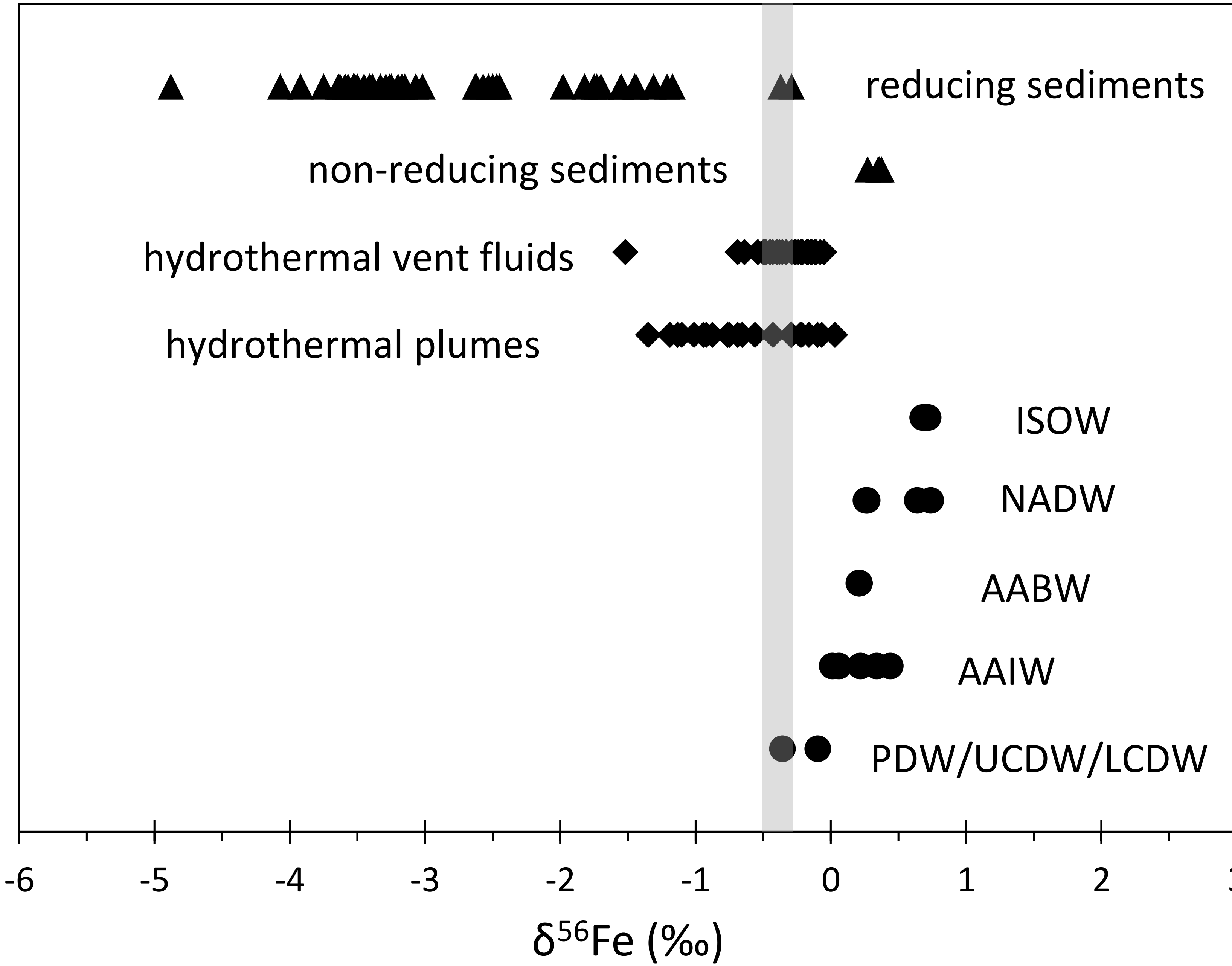
reducing sediments
non-reducing sediments
hydrothermal vent fluids
hydrothermal plumes
ISOW
NADW
AABW
AAIW
PDW/UCDW/LCDW
-6
-5
-4
-3
-2
-1
0
1
2
3
δ56Fe (‰)

Supplementary Information and Data Repository

Isotopic signature of dissolved iron delivered to the Southern Ocean from hydrothermal vents in the East Scotia Sea

Jessica K. Klar[1,2*], Rachael H. James[1], Dakota Gibbs[3,4], Alastair Lough[1], Ian Parkinson[5], J. Andrew Milton[1], Jeffrey A. Hawkes[6], and Douglas Connelly[2]

[1]*Ocean and Earth Science, University of Southampton Waterfront Campus, National Oceanography Centre Southampton, European Way, Southampton SO14 3ZH, UK*

[2]*Now at: LEGOS, University of Toulouse, IRD, CNES, CNRS, UPS, 18 av. Edouard Belin, 31401 Toulouse, France*

[3]*Marine Geosciences, National Oceanography Centre Southampton, European Way, Southampton SO14 3ZH, UK*

[4]*Southern Cross Geoscience, Military Road, Lismore, NSW 2480, Australia*

[5]*School of Earth Sciences, University of Bristol, Queens Road, Bristol, BS8 1RJ, UK*

[6]*Department of Chemistry, Uppsala University, SE-751 05 Uppsala, Sweden*

*Corresponding author; e-mail: Jessica.klar@legos.obs-mip.fr

STUDY AREA

The ESR is a back-arc spreading center located in the East Scotia Sea in the Atlantic sector of the Southern Ocean (Fig. S1). It is ~500 km long and consists of ten second-order ridge segments, from E1 in the north to E10 in the south, separated by non-transform faults.

Hydrothermal activity has been detected on segments E2 and E9 (German et al., 2000; Rogers et al., 2012).

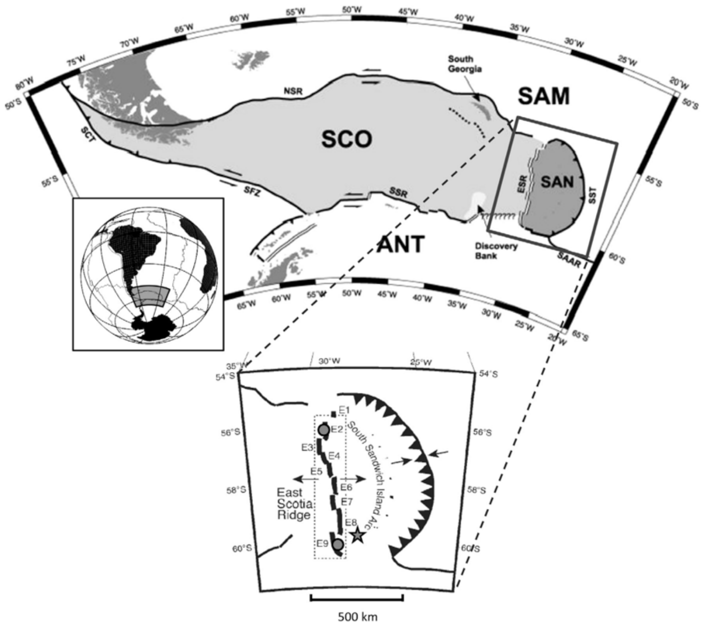

Figure S1. Location of the study area, showing the East Scotia Ridge (ESR) and the South Sandwich Island Arc. ESR segments E1 to E9 are labelled and vent fields at E2 and E9 are indicated by the grey circles. SAM: South American plate; ANT: Antarctic plate; SCO: Scotia plate; SAN: Sandwich plate; SFZ: Shackleton Fracture Zone; NSR: North Scotia Ridge; SSR: South Scotia Ridge; SCT: Southern Chile Trench; SST: South Sandwich Trench and SAAR: South American-Antarctic Ridge. Image from Cole et al. (2014).

Hydrothermal vent fluids from segment E2 have temperatures of up to 353 ºC (James et al., 2014) and low pH (~3.02), and endmember (zero Mg) concentrations of Fe and Mn range from, respectively, 790 to 1280 μM and from 2050 to 2220 μM. The chloride concentration of the endmember fluids (530 – 540 mM) is close to local bottom seawater (540 mM) and H_2S concentrations range from 6.7 to 7.1 mM (James et al., 2014). By contrast, vent fluids from the northernmost part of segment E9 (E9N) are hotter (up to 383 ºC) and the chloride concentration of the endmember fluid (98.2 mM) is distinctly lower than local bottom seawater, which is attributed to phase separation of the fluids (James et al., 2014). The pH of the vent fluids is between 3.08 and 3.42, and H_2S concentrations range from 9.5 to 14 mM. Concentrations of dFe in the endmember fluids (800 - 1210 μM) are similar to those measured at E2, whereas concentrations of dissolved Mn (~200 µM) are lower.

MATERIALS AND METHODS

Sample collection

Hydrothermal plumes were sampled on RRS *James Cook* cruises JC42 (2010, sampling of E2) and JC55 (2011, sampling of E9N). Hydrothermal plumes were detected and sampled using a SeaBird +911 CTD on a titanium (Ti) frame, equipped with up to 24 OTE (Ocean Testing Equipment) water sampling bottles, modified for trace metal sampling (fitted with external springs and Teflon taps; and metallic components replaced with Ti). A light scattering sensor (LSS) and a bespoke redox potential (Eh) detector were also mounted onto the frame. The buoyant part of the hydrothermal plume was identified by positive temperature and particle (LSS) anomalies and a negative Eh anomaly, and was located at ~2580 m water depth at E2 and ~2380 m water depth at E9N. The neutrally buoyant plume was identified by a positive particle anomaly and negative temperature and Eh anomalies at 250 – 300 m above the sea floor (~2300 m water depth at E2 and ~2150 m water depth at E9N) (Fig. S2).

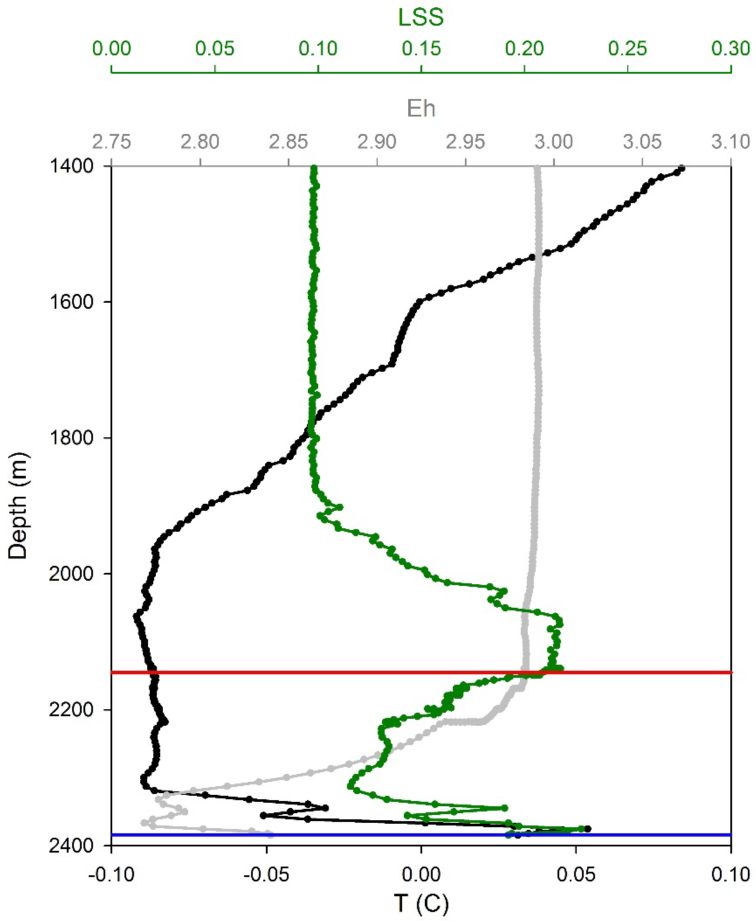

Figure S2. Representative temperature (T), LSS and Eh profiles for the lowermost part of the water column at E9N. Blue line indicates depth of samples collected from the buoyant plume and red line indicates the depth of samples collected from the neutrally buoyant plume. For profiles corresponding to E2 plumes see Hawkes et al., (2013).

Upon recovery of the CTD, the OTE bottles were transferred to the clean lab container on board and seawater samples were filtered through a polycarbonate membrane filter (0.2 µm, Whatman) under gentle pressure using filtered oxygen-free nitrogen gas and collected in 500 ml acid-cleaned LDPE bottles. After filtration of ~ 10 L of seawater, the filters were kept for particulate metals concentration analysis. All seawater samples were then acidified to approximately pH 1.9 with thermally distilled nitric acid (Optima, Fisher Scientific). Sample bottles were bagged and shipped back to the laboratory for isotopic analysis.

Vent fluids were sampled during cruise JC42 using titanium (Ti) syringe samplers mounted on the Remotely Operated Vehicle (ROV) Isis. These Ti syringe samplers were equipped with an inductively coupled link (ICL) temperature sensor at the nozzle tip. Once the ROV was recovered on board, the fluids were transferred into 1 L acid cleaned HDPE bottles. The samplers were acidified to pH < 2 using thermally distilled nitric acid and shipped back to the laboratory for analysis.

Sampling Artifacts

It is important to note that the partitioning of Fe between Fe(II) and Fe(III) and different size fractions within the samples does not necessarily correspond to the partitioning of Fe within the plume at the time of sampling, as oxidation of dFe may occur between the time of tripping the sampling bottles and filtration (Bennett et al., 2009). The average time interval between sampling the hydrothermal plumes and sample filtration on deck was > 5 hours, which corresponds to > 3 Fe(II) half-lives in surrounding waters, or < 0.6 Fe(II) half-lives in the more acidic buoyant plume (see 'Calculations of Fe(II) half-lives' below). This implies that there is high likelihood for continued oxidation of aqueous Fe(II) to Fe(III) and precipitation of Fe(III)-oxides within the OTE bottles during recovery. However, it is likely that oxidation rates in the OTE bottles are lower than calculated, as the bottles represent a closed rather than an open system. Although the buoyant plume samples contain a higher proportion of aqueous Fe(II) (see main text), they are also characterized by the slowest oxidation rates. As Fe sulfide precipitation and Fe(II) oxidation/Fe(III) precipitation occur in the early stages of vent fluid mixing with seawater, significant changes in redox speciation and size distribution of Fe, and therefore δ^{56}Fe, are unlikely, but cannot be ruled out.

Iron concentration and isotope analyses

All acids used for chemical processing of the samples were thermally distilled and regularly monitored for metal content. Milli-Q water was used for diluting acids and for cleaning. Low-density polyethylene (LDPE) sample bottles were cleaned for trace metal purposes using a three step cleaning procedure (2-3 days in 2.5 % Decon, 1 week in 50 % HCl and 1 week in 50 % HNO_3). The Teflon filtration unit (Savillex) used during the analytical procedure was cleaned in a similar manner, but the time in the acid baths was increased by a factor of 2. The unit was soaked in a 20 % HCl bath for at least a few hours between uses.

The concentration of dissolved metals (Fe and Mn) was determined by preconcentrating 100 ml of sample by mixed ligand extraction (Bruland et al., 1979), and analysis by inductively coupled plasma mass spectrometry (ICP-MS, Thermo Scientific X-Series). These results are reported in Hawkes et al. (2013). Fe concentrations were used to inform optimum isotope spiking. The concentration of Fe in the particulate size fraction was determined by ICP-MS, after digesting the polycarbonate filters for 3 days at 150 °C in sub-boiled concentrated nitric acid, followed by drying down and redissolution in 3 % sub-boiled nitric acid (Hawkes et al., 2013).

Iron isotopes in the dissolved fraction (0.2 μm filtered) of hydrothermal plume samples were analyzed at the NOC following a similar procedure to that reported in John and Adkins (2010). Briefly, a sub-sample (100 to 500 ml) was taken into an acid cleaned LDPE bottle, and Fe was preconcentrated from the seawater using a NTA resin batch method. The Fe fraction was then purified by anion exchange chromatography (AG1-X8 resin). The procedure blank, specific for these samples, was 2.5 ± 0.5 ng Fe (n = 6). Aliquots of vent fluid samples were oxidized by treatment with concentrated nitric acid and hydrogen peroxide before purification by anion exchange using AG-MP1 resin following Homoky et al., (2013). The procedure blank was 0.69 ± 0.05 ng Fe (n=2).

Isotopic measurements were carried out in duplicate on a multi-collector inductively coupled plasma mass spectrometer (MC-ICP-MS) (Thermo Scientific Neptune) at the NOC. Instrumental mass bias was corrected using a ^{57}Fe-^{58}Fe double spike, which was added to the samples before chemical processing. $^{56}Fe/^{54}Fe$ ratios are expressed as $\delta^{56}Fe$ relative to the average $^{56}Fe/^{54}Fe$ value for the iron isotope reference material IRMM-014 determined during the analytical session ($\delta^{56}Fe = [(^{56}Fe/^{54}Fe)_{sample}/(^{56}Fe/^{54}Fe)_{IRMM\text{-}14} - 1] \times 1000$). The external precision and accuracy were assessed by multiple analyses of two iron isotope standards. The average $\delta^{56}Fe$ of the ETH (Eidgenössische Technische Hochschule Zürich) standard was 0.52 ± 0.06 ‰ (2SD, n=191) and the average in-house HEM standard was 0.25 ± 0.06 ‰ (2SD, n=174). The ETH standard is within analytical uncertainty of the consensus value of 0.52 ± 0.08 ‰ (2SD, n=80; Lacan et al., 2010). The analytical Fe separation method was validated by taking ETH standard through the AG-MP1 purification procedure 0.55 ± 0.05 ‰ (n=2).

Additional analyses

Salinity (conductivity), temperature and depth (pressure) were measured for each water column profile using a Seabird CTD sensor mounted on the rosette frame. Discrete samples of seawater for salinity analysis were taken from selected OTE bottles on cruise JC055 to cross-calibrate the sensors and to identify miss-fired bottles. This was not done on JC042. The CTD was also equipped with calibrated light scattering (LSS), Eh and oxygen sensors.

CALCULATIONS AND ISOTOPE MODELLING

Calculation of vent fluid and buoyant plume dilution factors

The extent of dilution of the vent fluid by seawater (VF dilution factor; x-axis in Figure 1 in the main text) is calculated from the Mn concentration of the plume sample: *VF dilution factor* = $([Mn]_{VF} - [Mn]_{SW})/([Mn]_{sample} - [Mn]_{SW})$, where *[Mn]* represents the Mn concentration, *SW* represents background seawater, *VF* represents the end member vent fluid and *sample* represents the plume sample. $[Mn]_{VF} \approx 2050$ μM for E2 and $[Mn]_{VF} \approx 200$ μM for E9; $[Mn]_{SW} = 0.6$ nM (Table DR3). This calculation assumes that Mn behaves conservatively during mixing, due to its low reactivity and slow oxidation rate (Rudnicki and Elderfield, 1993).

Similarly, the extent of dilution of the buoyant plume (BP dilution factor; x-axis in Figure 3 of the main text) by surrounding seawater is calculated as: *BP dilution factor* = $([Mn]_{BP} – [Mn]_{SW})/([Mn]_{sample} – [Mn]_{SW})$, where *BP* represents the least dilute buoyant plume sample. $[Mn]_{BP} \approx 525$ nM for E2 and $[Mn]_{BP} \approx 34$ nM for E9N.

Calculation of Fe(II) half-lives

The Fe(II) half-life ($t_{1/2}=\ln 2/k_1$) in deep water masses surrounding E2 and E9 was calculated using the equations given in Millero et al., (1987):

$k_1 = k[O_2][OH^-]^2$ Eq. 1

$\log k = 21.56 - 1545/T - 3.29I0.5 + 1.52I$ Eq. 2

$I=19.9201S/(10^3-1.00488S)$ Eq. 3

Where k_1 is the pseudo first-order rate constant, k is the overall rate constant, $[O_2]$ is oxygen concentration in μmol/kg, $[OH^-]$ is hydroxide concentration in μmol/kg, T is temperature in degrees Kelvin, I is ionic strength and S is salinity. $[OH^-]$ was calculated from DIC and alkalinity measurements made on water samples collected during JC42 and JC55 (Hawkes et al., 2013), using the CO2Sys_v2.1 program (http://cdiac.ornl.gov/oceans/co2rprt.html). ESS deep water T, S and O_2 were obtained from WOA (https://www.nodc.noaa.gov/OC5/woa13/) stations 5481(B) and 3978(B). The Fe(II) half-life in waters surrounding E2 and E9 is 1.49 ± 0.10 hours (n = 16). The Fe(II) half-life is considerably longer (up to 8.5 h) in the slightly more acidic buoyant plumes at both sites.

Modelling of the isotopic fractionation during Fe(II) oxidation in the buoyant plume

Iron delivered by hydrothermal vents is initially in the reduced aqueous Fe(II) form (e.g., Statham et al., 2005). Immediately on venting at the seafloor, some of this iron precipitates as iron sulfides (e.g., Rudnicki and Elderfield, 1993) which leads to enrichment in heavier Fe isotopes of the remaining dFe, as described in the main text. Thus vent fluids that originally have δ^{56}Fe = -0.28 ‰ (E2) and δ^{56}Fe = -0.30 ‰ (E9N) have, respectively δ^{56}Fe values of +0.07 ± 0.05 ‰ (E2) and +0.49 ± 0.05 ‰ (E9N) after sulfide precipitation (see main text for details).

As the vent fluids mix with oxic seawater, Fe(II) starts to oxidize to aqueous Fe(III), which rapidly precipitates as Fe(III)-oxides. The Fe(III) preferentially incorporates heavier isotopes, leaving the remaining Fe(II) up to 3.56 ‰ lighter (Welch et al., 2003). The effect of Fe(II) oxidation on δ^{56}Fe can be modelled in terms of Raleigh distillation. Iron(II) is always in the dissolved phase and is considered to be the “vapor phase”, whereas Fe(III) that precipitates and leaves the “truly” dissolved phase is considered to be the “condensate phase” that is isolated from the aqueous Fe(II) species (i.e., equilibrium is not attained). The isotopic compositions of the remaining Fe(II) and the accumulated Fe(III) precipitate are therefore given by:

$$\delta^{56}Fe(II) = (\delta^{56}Fe(II)_0 + 1000) * f^{\alpha-1} - 1000 \qquad \text{Eq. 4}$$

$$\delta^{56}Fe(III) = \frac{1-f^{\alpha}}{1-f}(\delta^{56}Fe(II)_0 + 1000) - 1000 \qquad \text{Eq. 5}$$

where $\delta^{56}Fe(II)$ is the isotopic ratio of the remaining Fe(II), $\delta^{56}Fe(II)_0$ is the initial isotopic ratio of Fe(II) before oxidation starts (corrected for sulfide precipitation), $\delta^{56}Fe(III)$is the isotopic ratio of the accumulated precipitated Fe(III) and α is the fractionation factor between aqueous Fe(II) and precipitated Fe(III), $\alpha_{Fe(III)\text{-}Fe(II)}$ at a temperature of -0.09 °C (α=1.0036; Welch et al., 2003).

The Fe(III)-oxide particles are most likely distributed across a wide spectrum of particle sizes, including the colloidal size fraction (0.02 – 0.2 μm). Therefore, the dissolved size fraction (< 0.2 μm) is initially entirely composed of Fe(II), but as Fe(II) oxidation starts, an increasing proportion of the dissolved fraction will also consist of colloidal Fe(III) particles. As the Fe(III) aggregates into larger particles and leaves the dissolved size fraction, the isotopic composition of Fe remaining in the dissolved fraction is altered. Hence δ^{56}Fe of dFe delivered to the buoyant plume is modelled as a function of the fraction (*f*) of Fe remaining as Fe(II) and the proportion (*X*) of Fe(III) that remains in the dissolved (colloidal) phase:

$$\delta^{56}Fe = \frac{f*\delta^{56}Fe(II)+X*(1-f)*\delta^{56}Fe(III)}{f+X*(1-f)} \qquad \text{Eq. 6}$$

This model assumes that a constant proportion of Fe(III) is lost from the dissolved phase throughout the oxidation process. In reality, the rate of Fe(III)-oxide particle coagulation will vary over time, with highest rates at lowest plume dilution, where highest Fe and particle concentrations are found.

DATA REPOSITORY

Table S1. Concentrations of Mg, Mn and Fe and Fe isotopic compositions in high-temperature hydrothermal vent fluids sampled at vent sites E2 and E9N.

	Mg (mM)	Mn (µM)	Fe (µM)	δ^{56}Fe (‰)	2 SD (‰)
E2	1.64	2020	1066	-0.28	0.05
E9N	0.59	200	578	-0.30	0.05

Table S2. Sample locations, concentrations of dissolved and total (dissolved + particulate) Fe (tFe) and dissolved Mn (dMn), dFe isotopic composition and calculated vent fluid dilution factor in buoyant (grey shading) and neutrally buoyant plume samples.

Sample	Lat (°N)	Long (°E)	Depth (m)	VF Dilution factor	dMn (nM)	dFe (nM)	tFe (nM)	$\delta^{56}Fe$ (‰)	2 SD (‰)
E2, Cruise JC042									
3-01	-56.088	-30.319	2586	5900	348	36.1	144	-0.88	0.07
3-06	-56.088	-30.319	2574	3900	525	83.5	229	-1.19	0.11
3-07	-56.088	-30.319	2372	18000	112	20.2	N.D.	-0.75	0.06
3-11	-56.088	-30.319	2277	14000	147	30.9	50	-0.69	0.07
5-01	-56.089	-30.319	2567	5800	354	31.6	168	-1.10	0.07
7-02	-56.089	-30.318	2272	37000	56.4	12.1	18	-0.43	0.07
7-11	-56.089	-30.318	2272	21000	97.6	14.3	20	-0.66	0.10
7-13	-56.089	-30.318	2272	35000	58.3	18.0	24	-0.56	0.10
7-17	-56.089	-30.318	2272	28000	73.2	13.1	20	-0.29	0.07
E9N, Cruise JC055									
424-04	-60.043	-29.982	2382	7400	27.3	14.0	18	-0.23	0.09
424-07	-60.043	-29.982	2385	5800	34.8	23.0	27	-0.76	0.06
424-10	-60.043	-29.982	2144	35000	6.31	7.31	9	-0.29	0.05
424-14	-60.043	-29.982	2146	12000	10.6	10.9	17	-0.21	0.18

N.D: no data

Table S3. Concentration of dMn measured outside of the hydrothermal plumes in the East Scotia Sea. Average value = 0.6 ± 0.3 nM.

Sample	Lat (°N)	Long (°E)	Depth (m)	dMn (nM)
JC42-03-14	-56.088	-30.319	1000	0.28
JC42-04-17	-56.089	-30.318	2349	0.81
JC42-04-23	-56.089	-30.318	995	0.18
JC42-08-17	-56.089	-30.315	1000	0.40
JC42-10-18	-60.043	-28.982	1498	0.41
JC55-422-01	-59.682	-33.103	2350	0.96
JC55-422-02	-59.682	-33.103	2350	0.93
JC55-422-03	-59.682	-33.103	2350	0.30
JC55-422-13	-59.682	-33.103	2000	0.98
JC55-422-14	-59.682	-33.103	2000	0.20
JC55-422-15	-59.682	-33.103	2000	0.40
JC55-424-08	-60.043	-29.982	2218	0.69
JC55-424-22	-60.043	-29.982	1750	0.87

REFERENCES CITED

Bruland, K. W., Franks, R. P., Knauer, G. A., and Martin, J. H., 1979, Sampling and analytical methods for the determination of copper, cadmium, zinc, and nickel at the nanogram per liter level in sea-water: Analytica Chimica Acta, v. 105, no. 1, p. 233-245.

Cole, C. S., James, R. H., Connelly, D. P., and Hathorne, E. C., 2014, Rare earth elements as indicators of hydrothermal processes within the East Scotia subduction zone system: Geochimica et Cosmochimica Acta, v. 140, no. 0, p. 20-38.

German, C. R., Livermore, R. A., Baker, E. T., Bruguier, N. I., Connelly, D. P., Cunningham, A. P., Morris, P., Rouse, I. P., Statham, P. J., and Tyler, P. A., 2000, Hydrothermal plumes above the East Scotia Ridge: an isolated high-latitude back-arc spreading centre: Earth and Planetary Science Letters, v. 184, no. 1, p. 241-250.

Hawkes, J. A., Connelly, D. P., Gledhill, M., and Achterberg, E. P., 2013, The stabilisation and transportation of dissolved iron from high temperature hydrothermal vent systems: Earth and Planetary Science Letters, v. 375, no. 0, p. 280-290.

Homoky, W. B., John, S. G., Conway, T. M., and Mills, R. A., 2013, Distinct iron isotopic signatures and supply from marine sediment dissolution: Nat Commun, v. 4.

James, R. H., Green, D. R. H., Stock, M. J., Alker, B. J., Banerjee, N. R., Cole, C., German, C. R., Huvenne, V. A. I., Powell, A. M., and Connelly, D. P., 2014, Composition of hydrothermal fluids and mineralogy of associated chimney material on the East Scotia Ridge back-arc spreading centre: Geochimica et Cosmochimica Acta, v. 139, no. 0, p. 47-71.

John, S. G., and Adkins, J. F., 2010, Analysis of dissolved iron isotopes in seawater: Marine Chemistry, v. 119, p. 65-79.

Lacan, F., Radic, A., Labatut, M., Jeandel, C., Poitrasson, F., Sarthou, G., Pradoux, C., Chmeleff, J., and Freydier, R., 2010, High-Precision Determination of the Isotopic Composition of Dissolved Iron in Iron Depleted Seawater by Double Spike Multicollector-ICPMS: Analytical Chemistry, v. 82, no. 17, p. 7103-7111.

Millero, F. J., Sotolongo, S., and Izaguirre, M., 1987, The oxidation-kinetics of Fe(II) in seawater: Geochimica et Cosmochimica Acta, v. 51, no. 4, p. 793-801.

Rogers, A. D., Tyler, P. A., Connelly, D. P., Copley, J. T., James, R., Larter, R. D., Linse, K., Mills, R. A., Garabato, A. N., Pancost, R. D., Pearce, D. A., Polunin, N. V. C., German, C. R., Shank, T., Boersch-Supan, P. H., Alker, B. J., Aquilina, A., Bennett, S. A., Clarke, A., Dinley, R. J. J., Graham, A. G. C., Green, D. R. H., Hawkes, J. A., Hepburn, L., Hilario, A., Huvenne, V. A. I., Marsh, L., Ramirez-Llodra, E., Reid, W. D. K., Roterman, C. N., Sweeting, C. J., Thatje, S., and Zwirglmaier, K., 2012, The

Discovery of New Deep-Sea Hydrothermal Vent Communities in the Southern Ocean and Implications for Biogeography: Plos Biology, v. 10, no. 1.

Rudnicki, M. D., and Elderfield, H., 1993, A chemical model of the buoyant and neutrally buoyant plume above the TAG vent field, 26 degrees N, Mid-Atlantic Ridge: Geochimica et Cosmochimica Acta, v. 57, no. 13, p. 2939-2957.

Statham, P. J., German, C. R., and Connelly, D. P., 2005, Iron(II) distribution and oxidation kinetics in hydrothermal plumes at the Kairei and Edmond vent sites, Indian Ocean: Earth and Planetary Science Letters, v. 236, no. 3-4, p. 588-596.

Welch, S. A., Beard, B. L., Johnson, C. M., and Braterman, P. S., 2003, Kinetic and equilibrium Fe isotope fractionation between aqueous Fe(II) and Fe(III): Geochimica et Cosmochimica Acta, v. 67, no. 22, p. 4231-4250.